COMMUNICATIONS IN COMPUTATIONAL PHYSICS
Vol. **6**, No. 4, pp. 730-742

Commun. Comput. Phys.
October 2009

Effect of the Equilibrium Pair Separation on Cluster Structures

Y. Yang and D. Y. Sun*

State Key Laboratory of Precision Spectroscopy and Department of Physics, East China Normal University, Shanghai 200062, China.

Received 26 July 2008; Accepted (in revised version) 16 January 2009

Communicated by Xingao Gong

Available online 5 March 2009

Abstract. The effect of the equilibrium pair separation on the evolution of cluster structures is investigated based on a new proposed pair potential. The computational results demonstrate that the potential with large equilibrium pair separation stabilizes decahedra and close-packed structures, while disordered structures appear for the potential with small equilibrium pair separation. The icosahedral clusters are dominated in the middle range of equilibrium pair separation. For the small size clusters ($N \leq 24$) the dominated structural motif is the polytetrahedra, which is almost independent of the details of the potential.

PACS: 61.46.Bc, 36.40.Mr

Key words: Cluster structure, pair potential.

1 Introduction

Understanding the cluster structure represents one of the crucial issues in nanoscience. Exploring the novel structure of nanoclusters has brought a big challenge to traditional method and technique used widely for bulk condensed matters [1]. Up to date, few direct measurements of cluster structures are available experimentally [2], and much of the current theoretical understanding of cluster structures has been derived from atomic-scale molecular-dynamics (MD) and Monte Carlo (MC) simulations [3].

The computer simulations have been carried out on various systems. The model clusters, described by Lennard-Jones (LJ) and Morse potentials, have been studied extensively (e.g., [3]). Metal clusters are also widely studied using both density functional

*Corresponding author. *Email addresses:* 52060602010@ecnu.cn (Y. Yang), dysun@phy.ecnu.edu.cn (D. Y. Sun)

theory and classical many-body potentials (e.g., [3,5,6]). A few studies have extended to large molecule systems [7–17] and multi-element systems [18–26]. Over the past decades, many exotic structures, which are probably forbidden in bulk materials, have been reported. The excellent examples include the cage structures of carbon [27], the Icosahedral (*IH*) [28,29] and decahedral (*DH*) [30,31] atomic shell structures of metals, and the recent found cage structures of gold [32,33].

Many papers have reported the general structural effects of the different contributions to the interaction. For example, Doye and Wales found that the Friedel type oscillation in atomic potentials can strongly modulate the cluster structures [34–36]. The effect of the potential shape on the nature of disordered structure are also studied [37,38]. Baletto *et al.* have investigated crossover between different structural motifs (icosahedra, decahedra, and octahedra) for a few many-body potentials [39, 40]. Doye and Wales investigated the structural evolution for a set of Sutton-Chen families of potentials [41]. Gong and his coworkers have studied the relativistic effect on the structure of gold clusters, which leads to the finding of cage-like structures [32,33].

Since the shape of simple pair potential could be adjusted in a comprehensive way, pair potentials provide intuitive understanding of the general effects, *i.e*, the effect of potential shapes on cluster structures. Previously, the effect of the potential range and anisotropy on the cluster structures were studied for many simple pair potentials. Braier *et al.* have investigated six- and seven-atom Morse clusters over different interaction range [42]. A similar study was carried out on other model potentials [43,44]. Doye and Wales have made systematic studies on how the structure of Morse clusters changing with the interaction range. They found that the decrease of the interaction range results in destabilizing strained structures [7,45–48].

Although substantial efforts have been made by many researchers, the knowledge about the relationship between cluster structure and potential shape is still limited. The further studies along this line are needed. In this paper, the issue about how the equilibrium pair separation (d_{EPS}) affecting the cluster structure is studied. Physically, changing d_{EPS} corresponds to changing the effective size of atoms/molecules. The importance of the atomic/molecular size has been shown in recent studies on C_{60} [49]. Our current studies will shed light on the general effect of the equilibrium pair separation on the cluster structures.

The remainder of the paper is organized as follows. The following section describes the new model potential and the computational details. The cluster structures for a few selected parameters are presented in Section 3. The conclusions drawn from this work are summarized in Section 4.

2 Computational details

The potential we proposed is originally prompted by the effective pair potential [50] of many-body potential for iron [51,52], then we parameterize it into the current form:

$$\Phi(r)=\begin{cases} \varepsilon[\frac{r}{\sigma}-2.5]^3[\gamma-1.44719(\frac{\sigma}{r})], & r\leq 2.5\sigma, \\ 0, & r>2.5\sigma, \end{cases} \tag{2.1}$$

where ε and σ are energy and length unit respectively. r denotes the distance between atoms. γ is an adjustable parameter, which determines the d_{EPS} of the potential. The higher value of γ corresponds the smaller d_{EPS}. In current studies, ε is chosen to keep the potential well depth equal to one as γ changing. And σ equals to one for all case studied. Fig. 1 shows the new potential with a few selected γ of 0.8, 0.9, 0.95, 1.0, 1.05, 1.1 and 1.2. For comparing, the Morse and LJ potential, which have been fitted to have the same curvature at the bottom of the potential well, are also shown in this figure. Comparing with Morse and LJ potential, the new one is softer in repulsive part and stiffer in attractive part. From this figure, one can see that, the change of γ will directly adjust the equilibrium pair separation.

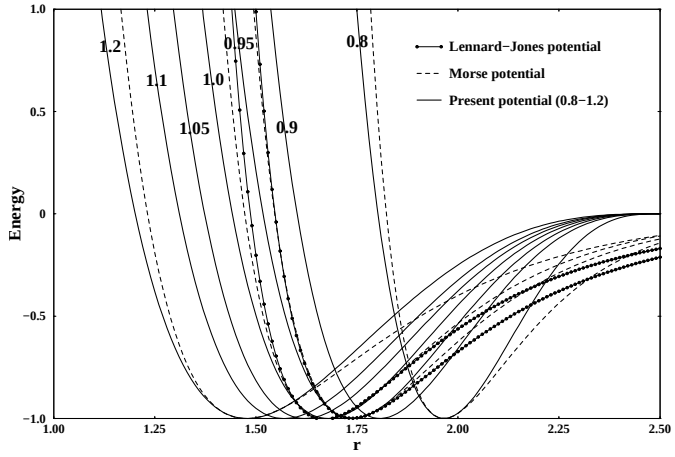

Figure 1: The new potential (solid line) for a few selected γ of 0.8, 0.9, 0.95, 1.0, 1.05, 1.1 and 1.2. For comparing, Morse (dashed line) and LJ (dotted-solid line) potential are also shown, which has been fitted to have the same curvature at the bottom of the potential well.

Another feature of the current potential is that, it can make both face-centered-cubic (fcc) and body-centered-cubic (bcc) structure stable by varying γ. Table 1 presents the cohesive energy of fcc and bcc phase for a few γ. Both fcc and bcc have the same cohesive energy at zero temperature at $\gamma=1$. For γ larger than one, bcc phase is more stable than fcc, while the smaller γ favors fcc phase. The reason is that, for large γ, the potential well becomes more and more flat. In this case, the dominated interaction in bcc is both first and second nearest neighbors totally 14 atoms, while only 12 first nearest neighbors are contributed to energy in fcc due to the limited interaction range. It needs to point that both Morse and LJ potential always make the fcc more stable than bcc. This is the major difference between the present potential and other pair potentials. This potential is also similar to the Johnson potential for bcc Iron [53], which implies that this form may represent major physics of bcc based metals.

Table 1: The cohesive energy of both fcc and bcc for different sets of γ, where ε is chosen so that the depth of potential well is 1.0. E_{bcc} and E_{fcc} are the cohesive energy for bcc and fcc structures respectively, and a_{bcc} and b_{fcc} are the equilibrium lattice constants for bcc and fcc structures respectively. For $\gamma<1.0$, fcc phase is more stable, while $\gamma>1.0$ bcc structure is more stable. At $\gamma=1.0$, fcc and bcc have the same cohesive energy.

γ	ε	E_{bcc}	E_{fcc}	a_{bcc}	a_{fcc}
0.80	98.496	-5.326	-6.000	2.222	2.778
0.90	29.415	-5.762	-6.000	2.036	2.557
0.95	18.760	-5.848	-6.001	1.932	2.457
1.00	12.786	-6.036	-6.036	1.859	2.361
1.05	9.168	-6.178	-6.124	1.793	2.264
1.10	6.844	-6.292	-6.252	1.730	2.176
1.20	4.172	-6.604	-6.547	1.589	2.021

To optimize the cluster structure, we first search for the global minimum among all the known structures for each potential and cluster size [54] using the steepest-descent method. Then we make further exploration for most stable structure with the generalized-simulated-annealing algorithm, which has been shown as a powerful and efficient method [55]. The most stable structure can then be found among these structures.

3 Results and discussions

Fig. 2 plots the second difference of energy ($\Delta_2E=E(N+1)+E(N-1)-2E(N)$) as a function of cluster sizes for all studied γ. From top to bottom, it corresponds to the value of γ from 0.8 to 1.2 respectively. For cluster size smaller than 25, all the curves have the same trend, which implies that structures are weakly dependent on the details of potentials. The similar case is also found for Morse potentials [48]. As the size larger than 24, the differences of these curves begin to emerge. The curve for $\gamma=0.8$ is evidently different from other γ. It is observed that $\gamma=0.9$ and 0.95 are similar to each other. A similar behavior is also found between $\gamma=1.0$ and 1.05, and between $\gamma=1.1$ and 1.2. For all γ except 0.8, Δ_2E is almost equal to zero for cluster size ranging from 135 to 146. The structure of these clusters are based on 147-atom icosahedron by removing one or more vertex atoms. Due to the short range of interaction and the symmetry among these vertex atoms, the energy change is almost the same by adding one vertex atom, which directly cause the zero of Δ_2E in this range.

Peaks in Δ_2E correspond to the specially stable clusters which have been found to correlated with magic numbers in mass spectra of clusters. We note that there are two types of peaks in Δ_2E. One type corresponds to specially stable clusters, namely the closed-shell *IH* structures of $N=13$, 55 and 147. Another kind is directly related to the change of structural types. For example, Δ_2E for $\gamma=0.8$ has several this type of peaks for $N>100$, which actually corresponds to the close-packed (*CP*) clusters changing to the *DH* motifs.

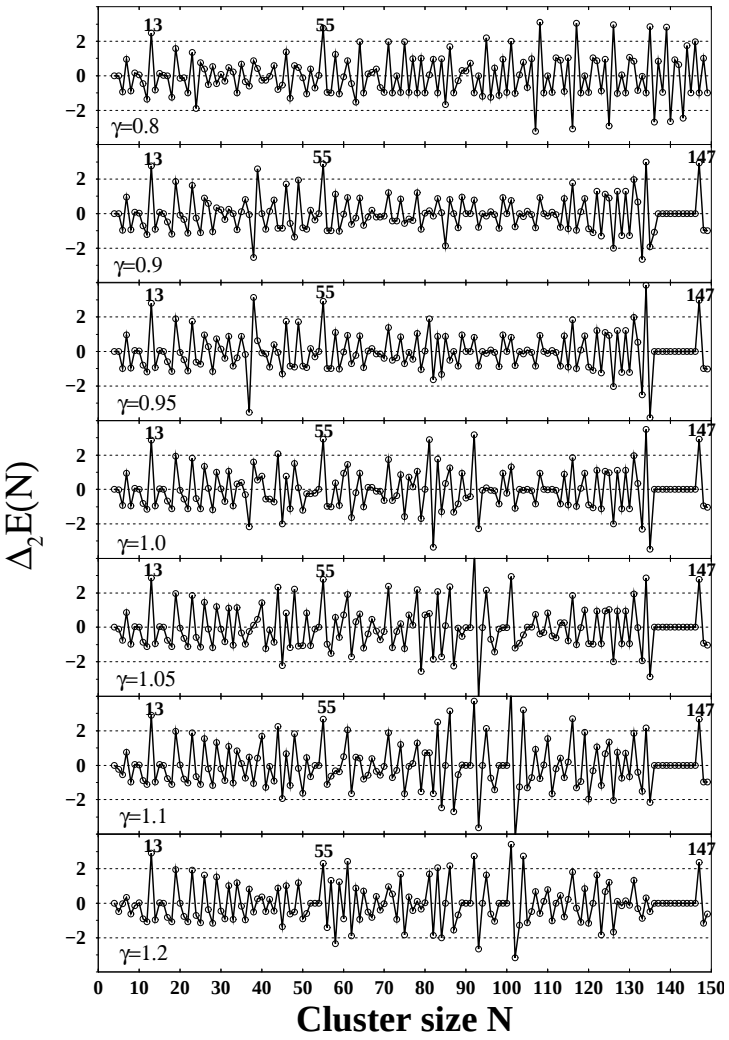

Figure 2: The second energy difference ($\Delta_2 E$) as a function of cluster size for all γ. Peaks in $\Delta_2 E$ correspond to clusters which are stable compared to adjacent sizes.

A few of structural types, *i.e*, polytetrahedra (*PT*), polytetrahedra involve an ordered array of disclinations (hereafter refers to *PT-d*), *IH*, *DH*, *CP* and disordered (*DIS*) structures, were found in present study. About these structures, the detailed description can be found elsewhere (e.g., [3] and references therein). Both *PT* and *PT-d* can be naturally divided up into tetrahedra with atoms at their corners. Most *PT* clusters are observed at small sizes. All clusters with number of atom less than 25 have *PT* type. More important, structures of them are identical for all γ at the same cluster size. This means that the cluster structures are weakly dependent on the details of potential. Fig. 3 shows *PT* clusters of $N=7-23$. The structural evolution of these *PT* cluster is based on the following mechanism: a $(N+1)$-atom cluster can be obtained by introducing new tetrahedra on the

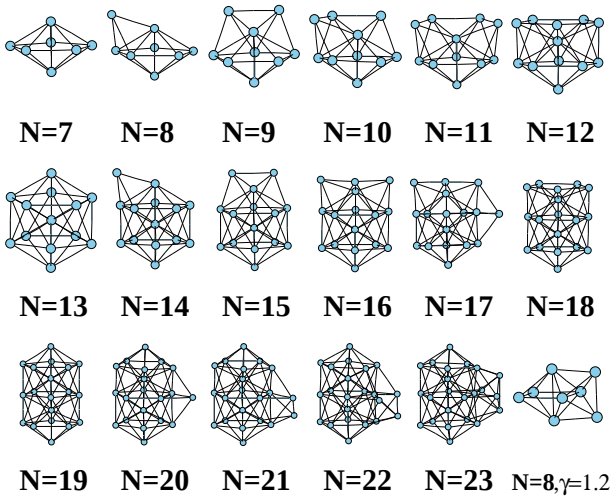

Figure 3: The small size polytetrahedral clusters of $N=7-23$. Most of them are identical for all γ at the same size. The exceptions are $N=8$ for $\gamma=1.2$.

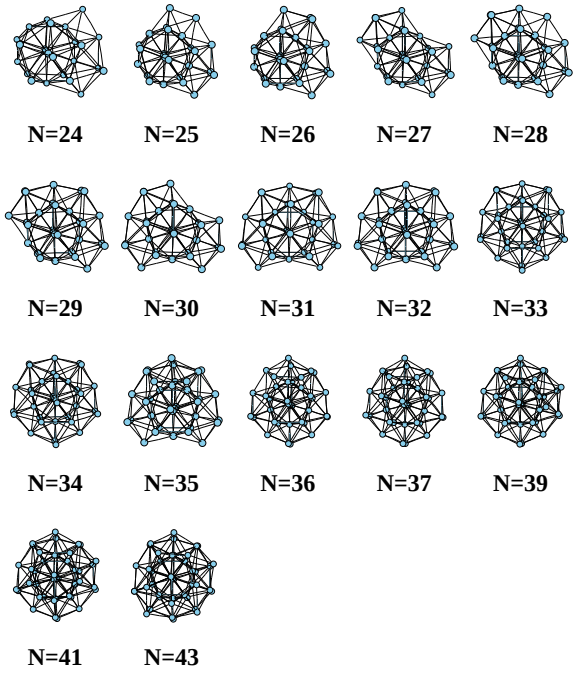

Figure 4: The extension of PT growth sequence based on the small PT clusters.

N-atom cluster. For example, the 7-atom cluster has a structure of pentagonal bipyramid, which can be viewed as packing of five small tetrahedra. By introducing more and more new tetrahedra, the 13-atom cluster can be formed. It needs to point out that, the struc-

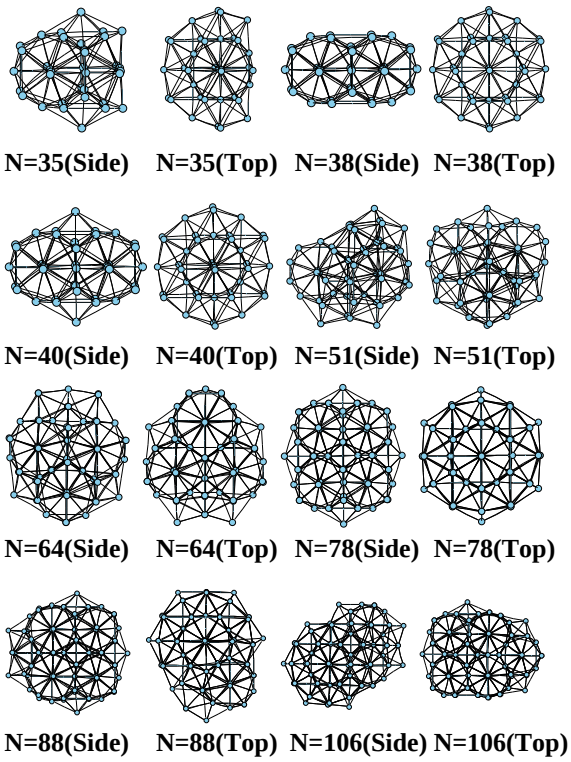

Figure 5: A few selected *PT-d* clusters.

ture of 13-atom cluster commonly regarded as an icosahedron, however, it is also a *PT* according to Hoare's description, and can be viewed as the packing of 20 small tetrahedra [56, 57]. Following the growth sequence, the large *PT* clusters can be constructed by packing more tetrahedra. Fig. 4 presents the *PT* cluster for $N=24$-43. The 8-atom cluster for $\gamma=1.2$ is similar to a fraction of bcc structure, which is different from the structure for the rest γ.

With increasing cluster size, the positive strain is also accumulated rapidly in *PT* clusters. To reduce the positive strain, *PT-d* structures are observed. This type of clusters has been discussed in several papers, e.g., [35, 47, 56]. Fig. 5 presents a few selected *PT-d* clusters, in which each cluster is given in the side view and the top view. These structures are different from *PT* by introducing six tetrahedra sharing one common edge. Although disclinations is unfavorable in local, it does result in the decrease of global strain of clusters. In fact, this structure is similar to the square-triangle Frank-Kasper phases for the quasi-crystals [58–61].

The *IH* clusters appear following the *PT-d* clusters at larger sizes. Some selected *IH* clusters are listed in the Fig. 6. Each cluster is given in the side view and the top view. There are many discussions in previous papers about *IH* [3]. Usually, comparing with *PT*

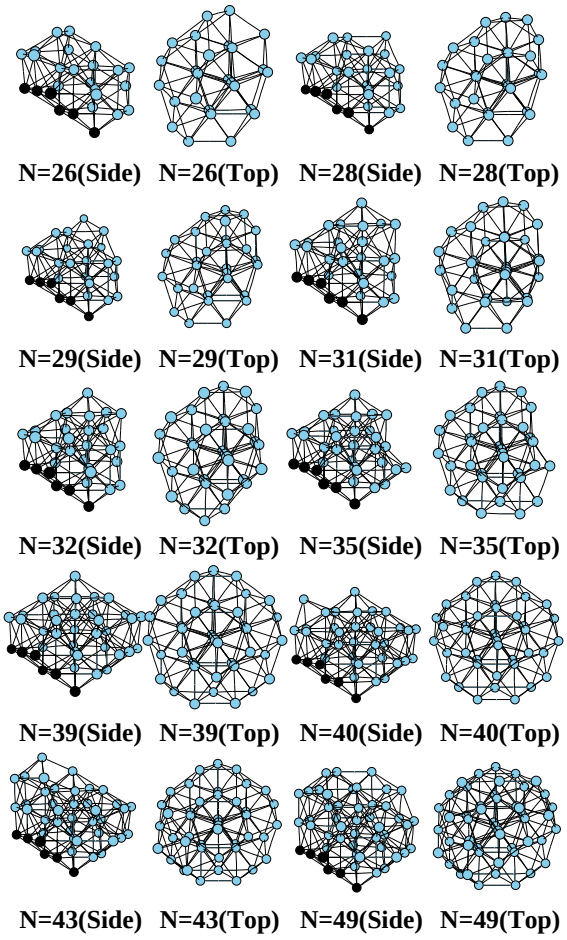

Figure 6: Some selected *IH* clusters. Each cluster presented in the side view and the top view, with a 6-atom fcc(111) surface marked in the side view, which is absent in *PT* and *PT-d* structures.

structure, *IH* structures have larger fcc(111) surface and atomic shell structure. For any *IH* based cluster, it can always form a closed-shell icosahedron by packing enough atoms on its surface. A few interesting *IH* clusters (see Fig. 7), which are not the fraction of nearest closed-shell *IH*, but the fraction of the larger icosahedron. For example, *IH* clusters with $N=48$ and 50 are not the fraction of 55-atom icosahedron, but the fraction of 147-atom icosahedron. A few clusters ($N=89$, 90 ($\gamma=0.8$), and $N=62$,65 ($\gamma=0.9-1.0$)) are the fraction of 561-atom icosahedron. These clusters were discussed by Baletto *et al.* [62] as natural pathway to the growth of larger *IH* clusters.

Fig. 8 shows some *DH*, *CP* and *DIS* structures. Both *DH* and *CP* clusters are found for the small value of γ. For simple pair potentials, the *DH* and *CP* structures can only exist for potential with very large d_{EPS}, such as C_{60} clusters. *CP* clusters have the same structure as fcc crystal, while *DH* is also more close to fcc structure over *PT* and *IH*. Disorder

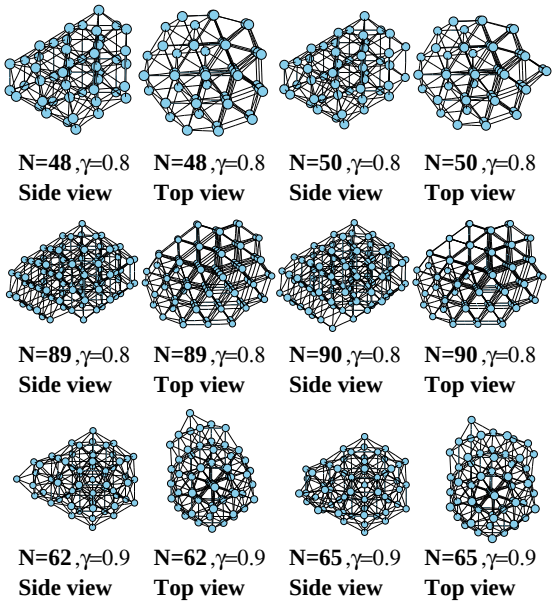

Figure 7: Some *IH* clusters are a fraction of larger closed-shell icosahedrons. The clusters with $N=48$ and 50 are the fraction of $N=147$ icosahedron; and $N=89$, 90 ($\gamma=0.8$) and $N=62$, 65 ($\gamma=0.9$-1.0) are the fraction of $N=561$ icosahedron.

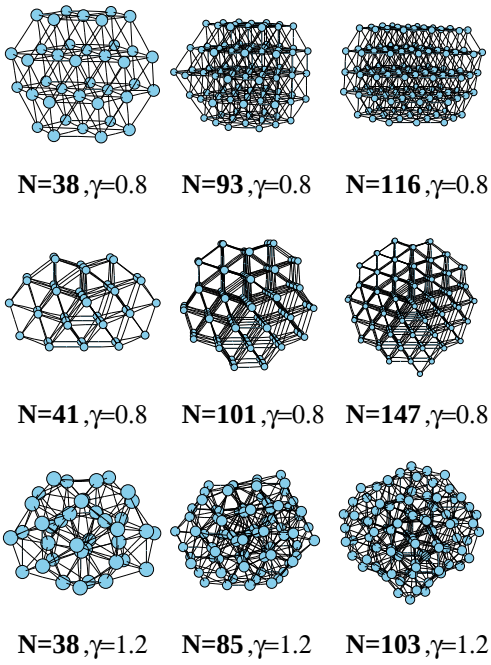

Figure 8: Some *DH*, *CP* and *DIS* clusters. Top row: *CP* clusters; Middle row: *DH* clusters; Bottom row: *DIS* clusters.

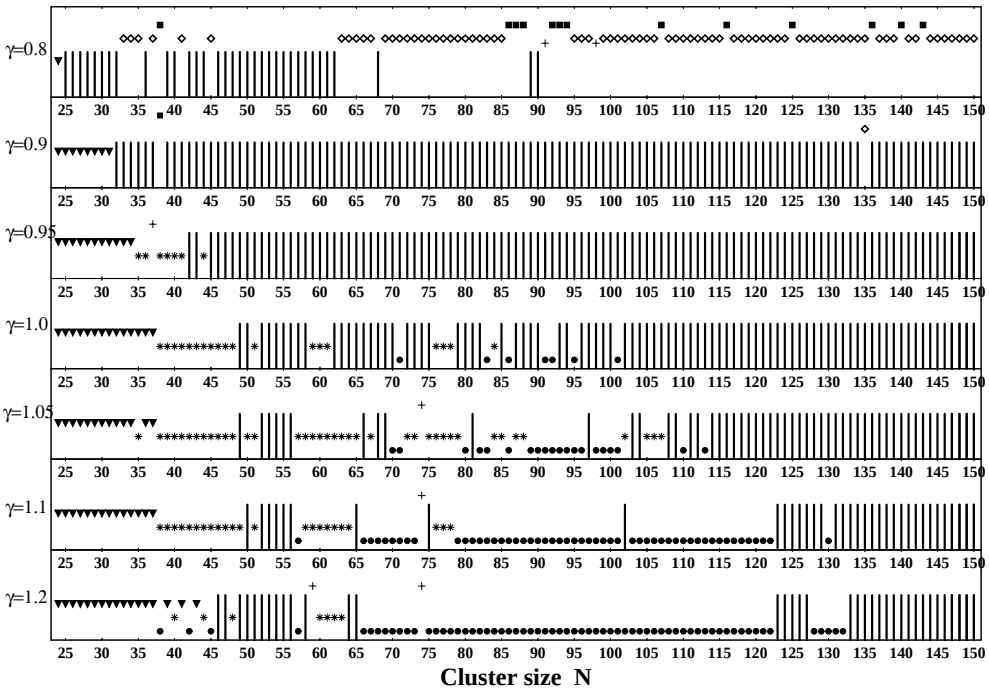

Figure 9: The zero temperature structural 'phase diagram' as a function of both size and γ. 'Filled triangles' for *PT*, 'Stars' for *PT-d*, 'Vertical lines' for *IH*, 'Filled squares' for *CP*, 'Open diamonds' for *DH*, 'Filled circles' for *DIS*, and 'Pluses' for some minor structure including interpenetrated clusters, a truncate tetrahedra ($N=91$, $\gamma=0.8$) [9], and a rare tetrahedron ($N=98$, $\gamma=0.8$) [63].

clusters appear for larger γ around 1.2, where the potential well is much flat. Some disordered clusters are in fact a serious distorted ordered structures. For example, distorted *IH* clusters ($N=85$, 103 for $\gamma=1.2$) are shown in Fig. 8. There are many disordered structures are hard to be recognized based on any ordered structures. Some interpenetrated clusters, which exhibit the combination of two type structures [47], are also found in the present studies. The interpenetrated clusters appear during the structure motif changing. For examples, the 59-atom cluster for $\gamma=1.2$ is found as an interpenetrated structure between *PT* and *IH*.

Fig. 9 plots structure 'phase diagram' as a function of both cluster size and γ at zero temperature. It can be seen that, the smaller γ, the more *DH* and *CP* clusters are, and the less *DIS* clusters are. For $\gamma=0.8$, the structure is dominated by the *DH* and *CP*. And only one *DH* and one *CP* clusters are found for the potentials with $\gamma\geq 0.9$. The number of *PT* clusters increase with increasing of γ. For different potentials, the largest size of *PT* clusters are $N=24$ for $\gamma=0.8$, $N=31$ for $\gamma=0.9$, $N=34$ for $\gamma=0.95$, $N=37$ for $\gamma=1.0$, 1.05, 1.1, and $N=43$ for $\gamma=1.2$. *PT-d* clusters are found in the size range from $N=25$ to 107. After the *PT-d* motif first emerges at $\gamma=0.95$, its number increases with the increase of γ, and reaches the maximum around $\gamma=1.05$. Further increasing γ, the distribution of *PT-d* motif begins to reduce. At $\gamma=1.2$, only seven *PT-d* clusters are found. The *DIS*

clusters first emerge at the large size between the two magic number $N=55$ and 147 at $\gamma=1.0$, and its distribution increase as the increasing of γ. At the value of $\gamma=1.2$, it is dominated by the disordered cluster. *IH* clusters dominate for $\gamma=0.9$ and 0.95, and its number decreases for both γ larger than 0.95 and smaller than 0.9.

Since clusters have non-negligible surface effect and large deformation comparing with bulk crystal, the competition between the deformation (strain) and surface effect plays the key role in determining cluster structures. According to this consideration, we can give a qualitative explanation for the 'phase diagram'. Small size clusters have very large surface-volume ratio, thus the surface effect is more important than the deformation. *PT* clusters are abundant at small sizes due to the low surface energy. For small size, *PT* structure can be broken only for strong atomic interaction [48]. To release the large strains in *PT* clusters, *PT-d* clusters appear with increase of size. Further increasing cluster sizes, both *PT* and *PT-d* become unfavorable, thus the *IH* clusters appear. *IH* clusters have the similar surface as *PT* and *PT-d*, but the inner strain is reduced when taking *IH* arrangement.

Among *IH*, *DH* and *CP* structure, *IH* structures have the lowest surface energy and largest deformation energy, *CP* structures are just the opposite, while *DH* is in the middle. For small γ (large d_{EPS}), the potential well becomes narrow, the small deformation (strain) will introduce large deformation energy, so *CP* and *DH* are dominated. For large γ (small d_{EPS}), the potential well becomes flat, correspondingly the deformation is less important, thus *IH* structures are favored. Obviously *DIS* structures have the largest deformation (strain), it should exist for much flat potential, this is the case of $\gamma=1.2$. The present results confirm the qualitative principle that decreasing the range of the pair-potential (the width of potential well) has the effect of destabilizing strained structures [45–48].

The most stable structure of bulk phase is bcc for $\gamma>1.0$, however only one cluster seems like a fraction of bcc, which is the cluster with $N=8$ for $\gamma=1.2$. On the contrary, a large number of *IH* and *PT* clusters are found for $\gamma>1.0$. The main reasons may be the surface effect, which results in the clusters adopting the fcc(111) surface. However, there could be the inherent competition between fcc and bcc, the existence of *DIS* clusters could be the consequence for $\gamma>1.0$.

4 Summary

In this paper, we have studied how the change of equilibrium pair separation modulates the structure of atomic clusters. For this purpose, a simple pair potential whose equilibrium pair separation can be varied under a fixed interaction range has been proposed. This potential can also stabilize both face-centered-cubic and body-centered-cubic structure by changing one of the parameters. By systematically seeking the ground state for each size and potential, the 'phase-diagram' is obtained. The 'phase-diagram' shows that both *PT* and *PT-d* structures are only presented for small size. *DH* and *CP* are presented for potential with large equilibrium pair separation, while disordered clusters appear for

the potential with small equilibrium pair separation. For the middle range of equilibrium pair separation, the *IH* structures are found dominated.

Acknowledgments

This research was supported by the National Science Foundation of China and Shanghai Project for the Basic Research. The computation is performed in the Supercomputer Center of Shanghai.

References

[1] H. S. Nalwa, Encyclopedia of Nanoscience and Nanotechnology (American Scientific, New York, 2004).
[2] L. D. Marks, Rep. Prog. Phys. 57, 603 (1994).
[3] F. Baletto and R. Ferrando, Rev. Mod. Phys. 77, 371 (2005).
[4] D. J. Wales, Energy Landscapes with Applications to Clusters, Biomolecules and Glasses (Cambridge University, Cambridge, England, 2003).
[5] R. C. Longo, E. G. Noya and L. J. Gallego, J. Chem. Phys. 122, 226102 (2005).
[6] R. C. Longo, E. G. Noya and L. J. Gallego, Phys. Rev. B 72, 174409 (2005).
[7] J. P. K. Doye and D. J. Wales, Chem. Phys. Lett. 247, 339 (1995).
[8] J. P. K. Doye and D. J. Wales, Chem. Phys. Lett. 262, 167 (1996).
[9] J. P. K. Doye, D. J. Wales, W. Branz and F. Calvo, Phys Rev. B 64, 235409 (2001).
[10] J. Hernández-Rojas, J. Bretón, J. M. Gomez Llorente and D. J. Wales, J. Chem. Phys. 121, 12315 (2004).
[11] J. Hernández-Rojas, J. Bretón, J. M. Gomez Llorente and D. J. Wales, J. Phys. Chem. B, 110, 13357 (2006).
[12] M. P. Hodges and D. J. Wales, Chem. Phys. Lett. 324, 279 (2000).
[13] S. Maheshwary, N. Patel, N. Sathyamurthy, A. D. Kulkarni and S. R. Gadre, J. Phys. Chem.-A 105, 10525 (2001).
[14] D. J. Wales and M. P. Hodges, Chem. Phys. Lett. 286, 65 (1998).
[15] H. M. Lee, S. B. Suh, and K, S, Kim, J. Chem. Phys. 115, 7331 (2001).
[16] T. James, D. J. Wales and J. Hernández-Rojas, Chem. Phys. Lett. 415, 302 (2005).
[17] B. S. González, J. Hernández-Rojas, D. J. Wales, Chem. Phys. Lett. 412, 23 (2005).
[18] J. Jellinek and E. B. Krissinel, Chem. Phys. Lett. 258, 283 (1996).
[19] G. Rossi, A. Rapallo, C. Mottet, A. Fortunelli, F. Baletto and R. Ferrando, Phys. Rev. Lett. 93, 105503 (2004).
[20] D. Sabo, J. D. Doll and D. L. Freeman, J. Chem. Phys. 121, 847 (2004).
[21] A. Rapallo et al., J. Chem. Phys. 122, 194308 (2005).
[22] J. P. K. Doye and L. Meyer, Phys. Rev. Lett. 95, 063401 (2005).
[23] R. Ferrando, A. Fortunelli and G. Rossi, Phys. Rev. B 72, 085449 (2005).
[24] R. C. Longo, E. G. Noya and L. J. Gallego, J. Chem. Phys. 122, 083311 (2005).
[25] R. C. Longo, E. G. Noya, A. Vega and L. J. Gallego, Solid State Commun. 140, 480 (2006).
[26] B. C. Curley, G. Rossi, R. Ferrando and R. L. Johnston, Eur. Phys. J. D 43, 53 (2007).
[27] H. Kroto, J. Heath, S. O'Brien, R. Curl and R. Smalley, Nature 318, 162 (1985).
[28] A. L. Mackay, Acta Crystallogr. 15, 916 (1962).

[29] T. P. Martin, Phys. Rep. 273, 199 (1996).
[30] S. Ino, J. Phys. Soc. Jpn. 27, 941 (1969).
[31] L. D. Marks, Philos. Mag. A 49, 81 (1984).
[32] X. Gu, M. Ji, S. H. Wei, X. G. Gong, Phys. Rev. B 70, 205401 (2004).
[33] M. Ji, X. Gu, X, Li, X. G. Gong, J. Li, L. S. Wang, Angew. Chem. Int. Edit. 44, 7119 (2005).
[34] J. P. K. Doye, D. J. Wales and S. I. Simdyankin, Faraday Discuss. 118, 159 (2001).
[35] J. P. K. Doye and D. J. Wales, Phys. Rev. Lett. 86, 5719 (2001).
[36] J. P. K. Doye, D. J. Wales, F. H. M. Zetterling and M. Dzugutov, J. Chem. Phys. 118, 2792 (2003).
[37] J. M. Soler, M. R. Beltrán, K. Michaelian, I. L. Garzón, P. Ordejón, D. Sánchez-Portal and E. Artacho, 2000, Phys. Rev. B 61, 5771 (2000).
[38] J. P. K. Doye, Phys. Rev. B 68, 195418 (2003).
[39] F. Baletto, R. Ferrando, A. Fortunelli, F. Montalenti and C. Mottet, J. Chem. Phys. 116, 3856 (2002).
[40] K. Michaelian, N. Rendón and I. L. Garzón, Phys. Rev. B 60, 2000 (1999).
[41] J. P. K. Doye and D. J. Wales, New J. Chem. 22, 733 (1998).
[42] P. A. Braier, R. S. Berry and D. J. Wales, J. Chem. Phys. 93, 8745 (1990).
[43] C. Rey and L. J. Gallego, Phys. Rev. E 53, 2480 (1996)
[44] C. Amano, M. Komuro, S. Mochizuki, H. Urushibara and H. Yamabuki, J. Mole. Struct.:THEOCHEM 758, 41 (2006).
[45] J. P. K. Doye and D. J. Wales, J. Phys. B 29, 4859 (1996).
[46] J. P. K. Doye and D. J. Wales, Science 271, 484 (1996).
[47] J. P. K. Doye and D. J. Wales, J. Chem. Soc. Faraday Trans. 93, 4233 (1997).
[48] J. P. K. Doye, D. J. Wales and R. S. Berry, J. Chem. Phys. 103, 4234 (1995).
[49] M. H. J. Hagen, E. J. Meijer, G. C. A. M. Mooij, D. Frenkel and H. N. W. Lekkerkerker, Nature 365, 425 (1993).
[50] A. E. Carlsson, Solid State Phys. 43, 1 (1990).
[51] G. J. Ackland, D. J. Bacon, A. F. Calder and T. Harry, Philos. Mag. A 75, 713 (1997).
[52] M. I. Mendelev, S. Han, D. J. Srolovitz, G. J. Ackland, D. Y. Sun and M. Asta, Philos. Mag. 83, 3977 (2003).
[53] R. A. Johnson and D. J. Oh, J. Mater. Res. 4, 1195 (1989).
[54] The Cambridge Cluster Database, D. J. Wales, J. P. K. Doye, A. Dullweber, M. P. Hodges, F. Y. Naumkin F. Calvo, J. Hernández-Rojas and T. F. Middleton, URL: `http://www-wales.ch.cam.ac.uk/CCD.html`.
[55] Y. Xiang, D.Y. Sun, W. Fan and X.G. Gong, Phys. Lett. A 233, 216 (1997).
[56] J. P. K. Doye, J. Chem. Phys. 119, 1136 (2003).
[57] M. R. Hoare and P. Pal, Adv. Phys. 20, 161 (1971).
[58] F. C. Frank and J. S. Kasper, Acta Crystallogr. 11, 184 (1958).
[59] F. C. Frank and J. S. Kasper, Acta Crystallogr. 12, 483 (1959).
[60] D. P. Shoemaker and C. B. Shoemaker, Introduction to Quasicrystals, edited by M. V. Jaric (Academic, London, 1988), pp. 1-57.
[61] D. Shechtman, I. Blech, D. Gratias and J. W. Cahn, Phys. Rev. Lett. 53, 1951 (1984).
[62] F. Baletto, C. Mottet and R. Ferrando, Phys. Rev. B 63, 155408 (2001).
[63] R. H. Leary, and J. P. K. Doye, Phys. Rev. E 60, R6320 (1999).